The Stress and the Earth Pressure Phenomena in the Rocks around Shaft Bottom Spaces

AUTHOR(S):

HIRAMATSU, Yoshio; OKA, Yukitoshi

CITATION:

HIRAMATSU, Yoshio ...[et al]. The Stress and the Earth Pressure Phenomena in the Rocks around Shaft Bottom Spaces. Memoirs of the Faculty of Engineering, Kyoto University 1963, 25(2): 188-202

ISSUE DATE:

1963-09-20

URL:

http://hdl.handle.net/2433/280560

The Stress and the Earth Pressure Phenomena in the Rocks around Shaft Bottom Spaces

By

Yoshio HIRAMATSU* and Yukitoshi OKA*

(Received January 31, 1963)

In general, shaft bottom spaces in mines are large and of complex shape, and are the most important places for haulage and winding. Though it is essential to clear up the earth pressure phenomena around these spaces in order to plan rational linings, very few investigations have been carried out into this problem. The authors have, therefore, studied the stress and the earth pressure phenomena around shaft bottom spaces by means of barodynamics and three dimensional photoelastic experiments. In the latter experiments, special consideration has been given to the treatment of statically indeterminate stresses.

It is found, from this study, that if the rock is not sufficiently strong, failure takes place on the roof, especially at the part of the roof between a shaft and a horizontal level, due to tensile stress, and in a few cases on the side walls due to compressive stress; that the degree of stress concentration is not so high as expected; and that these failures do not progress further once the corners of rock have been rounded off. Furthermore, there is a discussion of how to line the shaft bottom spaces.

1. Introduction

The shaft bottom space where a haulage level connects with a shaft is one of the most important places in a mine, and it must be kept for a long period of time without any deformation. In coal mines, the rocks in which such spaces are made are comparatively weak stratified rocks. Moreover, the shafts recently sunk in Japanese coal mines are mostly deep and the shaft bottom spaces are large and of complex shape. Therefore, it has become a subject for study to investigate how to support the rock around such spaces. Accordingly, the authors have studied, first, the probable failure of rock around a shaft bottom space by barodynamics, and second, they have investigated the stress in the rock by three-dimensional photoelastic experiments. Also, the variation in the stresses in the linings constructed for some shaft bottom spaces recently excavated has been measured. The present paper describes the details of these investigations.

* Department of Mining Engineering

2. Barodynamic experiments

(1) Purpose

Barodynamic experiments belong to a variety of model experimentation. In these experiments models are subjected to centrifugal force of such an intensity that the force gives rise to similar phenomena in the models as those caused by gravity in the prototypes. The chief purpose of the present experiments is to investigate in what part and in what manner the rock around shaft bottom spaces will fail when the rock is not sufficiently strong, and to find, if possible, on what conditions such a failure will take place.

(2) Method of experiments

Models. Models of two kinds of shaft bottom spaces, 174 mm long, 73 mm wide and 126 mm high, were made of weak cement mortar, the shapes and dimensions of which being illustrated in Fig. 1. The vertical circular hole in the model corresponds to a shaft, while the horizontal circular hole a haulage level. Fine sand, −28～+65 mesh, was used for the mortar and its mix proportion was 1 : 10, its water cement ratio 100%. The tensile and compressive strengths were tested for each model when it was subjected to the barodynamic experiment.

Equipment for the experiments. The equipment for the experiment consists of a centrifuge, a driving apparatus and a stroboscope for observation[1]. The centrifuge has a rotating frame, 50 cm long, 14 cm wide, 28 cm high, to which two models of the same construction are attached.

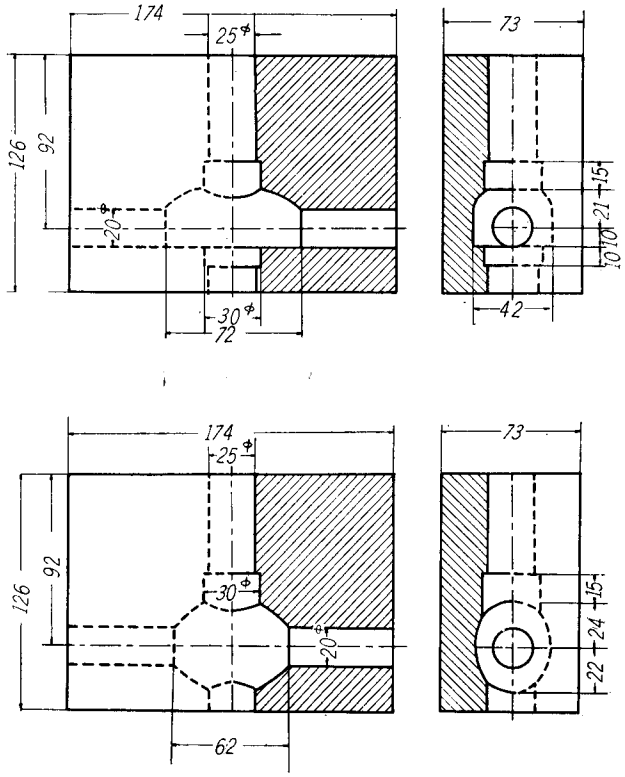

Fig. 1. The shapes and dimensions of the Model Type A and Model Type B. (Uunit : mm)

The frame is rotated at any optional speed, up to about 3000 r.p.m.. At the highest speed, centrifugal acceralation of about 2600 times the acceralation of gravity is applied to models. In order to be able to adjust the number of revolutions smoothly, the driving apparatus is of the Ward Leonard type constructed with a 5 HP 3 phase AC motor, a 110 V 5 HP DC generator, a 110 V 1 HP exciter and a 3 HP Ward Leonard motor.

Procedures of the experiments. The experiments were carried out in the following way. Each model was attached to the rotating frame of the centrifuge and rotated. The revolutions per minute were increased step by step, and the phenomena caused by centrifugal force was carefully observed by suspending operation of the centrifuge after 3 minutes of running at every step. This procedure was continued until considerable failure occurred around the shaft bottom space. From these experiments, we can see, at once, where and what failure takes place around the space.

Discussion. As the theory about barodynamics has been frequently described in several papers[2], it will be unnecessary to repeat it here. Let us show, therefore, its essentials only. Let the dimension ratio, the stress ratio and the density ratio of the prototype to the model be λ, μ and ν respectively, and the distance of a point in a model from the axis of the rotating frame be r, the revolutions per unit time be n. Then there exists the following relation.

$$\mu = \lambda\nu g/4\pi^2 r n^2 . \qquad (1)$$

In models, the body force per unit volume varies with the depth from the surface, whereas in the prototype it is almost constant. Taking account of this fact, it is proved that the distance r in Eq. (1) is to be taken as $r_0+h/2$, where r_0 is the distance of the surface of a model from the axis of the rotating frame and h the depth of a point concerned from the surface of a model[1]. See Fig. 2.

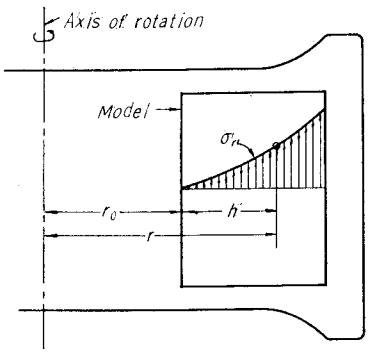

Fig. 2.

We can find the undisturbed stress, σ_k kg/cm^2, at the depth of the shaft bottom space in the models at the moment when the failure begins, from the density ρ kg·s^2/cm^4, the depth h cm, the number of revolutions per second n s^{-1} and the distance of the surface of a model from the axis of rotation r_0 cm, by Eq. (2).

$$\sigma_k = \rho h(2\pi n)^2(r_0+h/2) . \qquad (2)$$

In barodynamic experiments relating to the earth pressure phenomena around shaft bottom spaces, however, the proportion of the dimensions of the spaces to their depths in the models are, inevitably, far greater than that in the prototype, and it is impossible to apply proper side pressure to models. Furthermore, the condition of failure of the material composing the models is, in general, not the same as that of the rock. Under these circumstances, it is difficult to draw quantitative conclusions as to the failure of rock around shaft bottom spaces from barodynamic experiments, though the stress ratio of the prototype and models can be evaluated with Eq. (1).

Thus, in order to discuss the conditions for failure of rock around shaft bottom spaces, models of another kind having only a circular horizontal level in each one were produced of the same material, and they were subjected to barodynamic experiments. By comparing the revolution speed at which these models failed with that at which the models of shaft bottom spaces failed, we guessed in what degree the rock around a shaft bottom space is likely to fail.

(3) Results obtained

It was found that when the revolution speed reached a certain limit, such parts of the roof of a shaft bottom space that were on the haulage level side

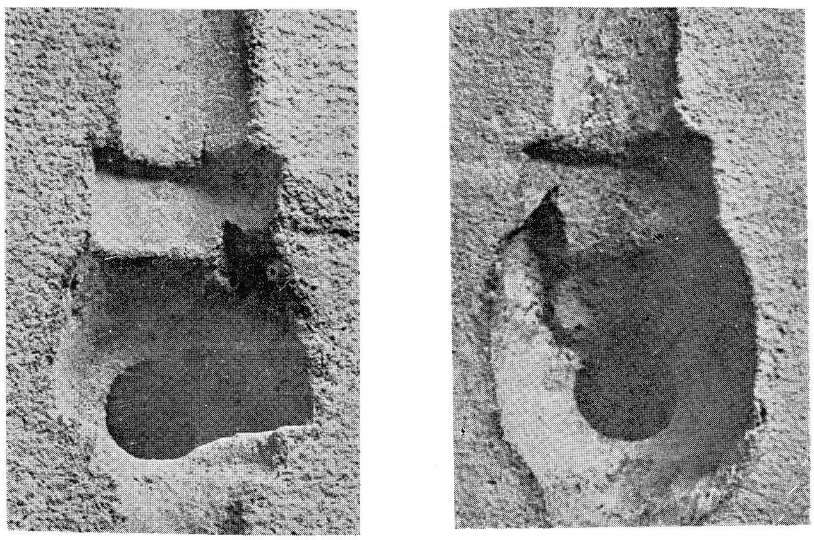

Type A　　Type B

Fig. 3-a. Photographs showing the failures seen on one Model Type A and on one Model Type B that were cut vertically through the axes of the shafts.

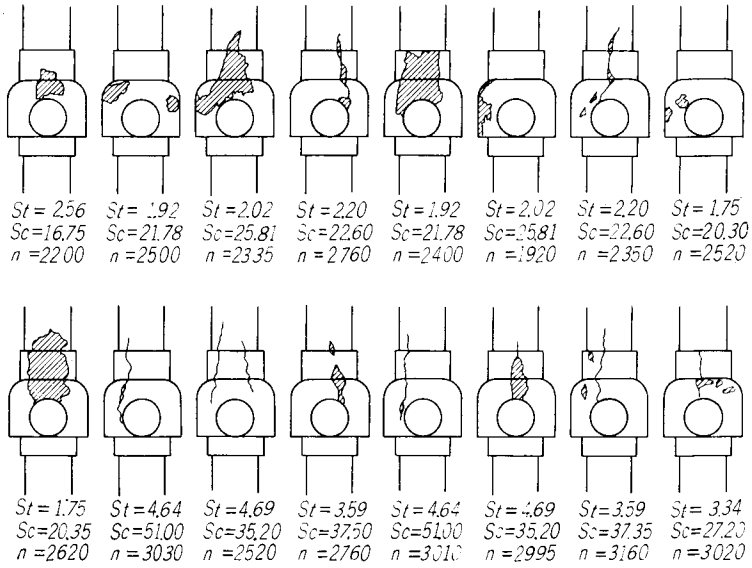

Models Type A

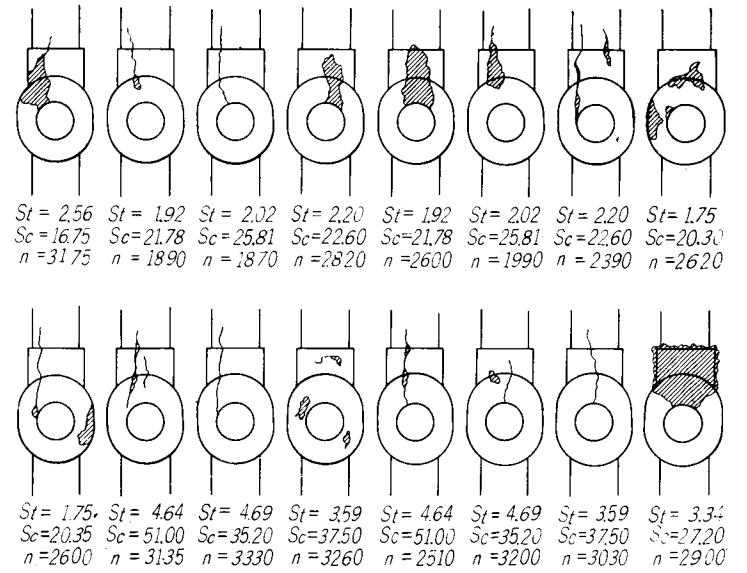

Models Type B

Fig. 3–b. The failures seen on all the tested models cut vertically through the axes of the shafts. (s_t: Tensile strength in kg/cm^2, s_c: compressive strength in kg/cm^2 and n: number of revolutions per minute.)

began to fall, but this failure did not progress very much. It seemed that the failure is due to concentrated tensile stress. Sometimes the side walls of the space fell slightly, owing to, perhaps, concentrated compressive stress. Figs. 3-a and b show the aspect of the failure that was seen on the tested models cut vertically through the axes of the shafts.

It is supposed that around the shaft bottom spaces there appear concentrated tensile or compressive stresses, which cause failure when they reach the tensile or compressive strength, s_t or s_c, of the material of the models. The ratio of s_t or s_c to σ_k may be taken as an index showing how the rock is likely to fail. As mentioned before, σ_k is given by Eq. (2).

From the results of experiments shown in Fig. 3, we see that s_t/σ_k is 0.36 for models Type A and 0.29 for models Type B. From the experiments with the models having circular horizontal levels, we find the value of s_t/σ_k to be about 0.11 for these models. The cause of failure is supposed to be the concentrated tensile stress for both the models. It is concluded, therefore, that rock around shaft bottom spaces shaped like the models Type A and B is likely to fail somewhat more frequently than that around a circular horizontal level if the rocks around both openings are of the same nature and strength.

3. Photoelastic experiments

In order to determine quantitatively the stress around shaft bottom spaces excavated in ground under several states of stress, photoelastic experiments were carried out.

(1) Method of experiments

Models. Two kinds of models were subjected to three-dimensional photoelastic experiments. The shapes of the models, 15 cm × 15 cm × 15 cm, are as shown in Fig. 4. The model Type C has an opening like that in the model Type A, while the opening in the model Type D has such a shape that every corner found around the opening in the model Type C is rounded off.

Every model was produced by casting epoxy resin into a metal box in which an inner mold of marble, as shown in Fig. 5, that has just the same shape as the open space to be made in the model was fixed, and by dissolving out the marble mold in hydrochloric acid after the resin became hard. The models thus produced were annealed by heating them at 130°C for 48 hours to eliminate residual stresses. Fig. 6 shows one of the models.

In order to test the photoelastic sensitiveness, a tension test piece, 14 cm × 3 cm × 1.4 cm, was made of the same material for each model.

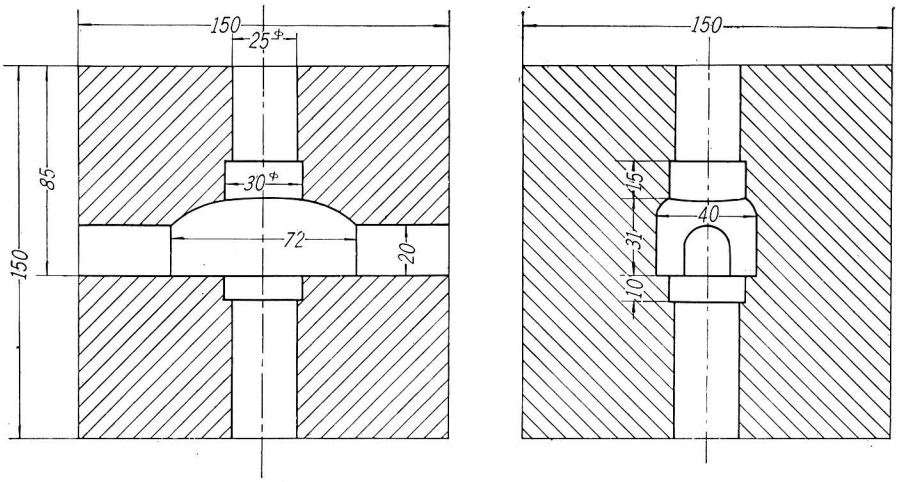

Model Type C

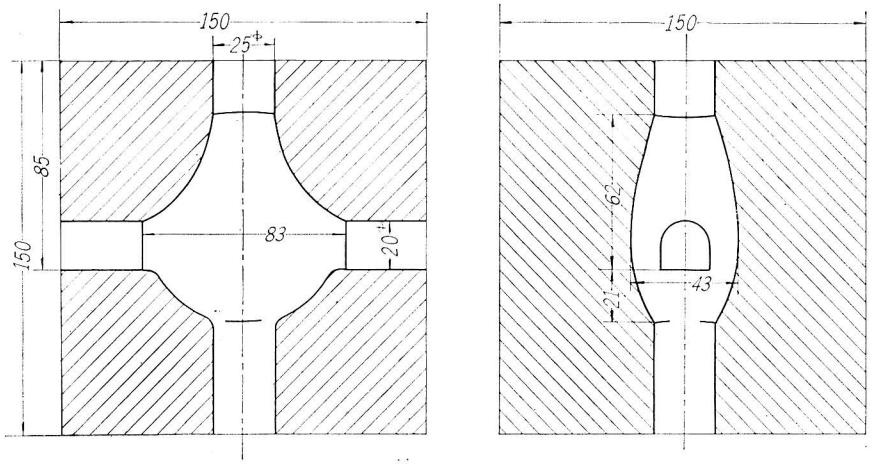

Model Type D

Fig. 4. The shapes and dimensions of the Model Type C and Model Type D. (Unit : mm)

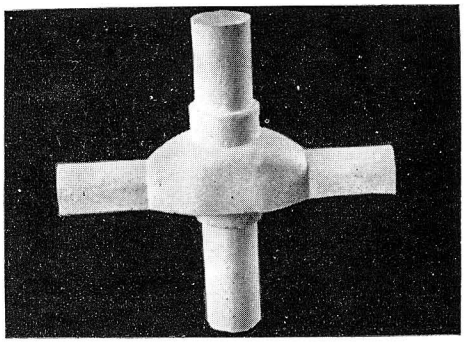

Fig. 5. An inner mold of marble for the open space in the Model Type C.

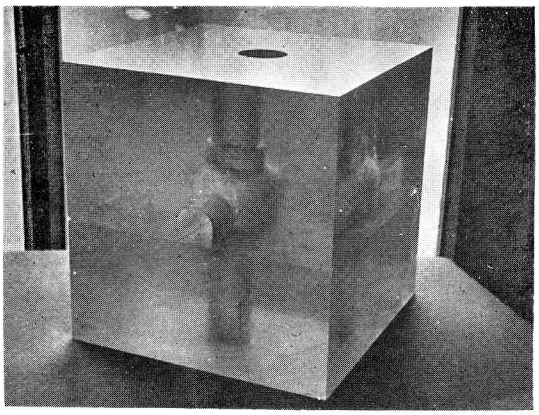

Fig. 6. Model Type C.

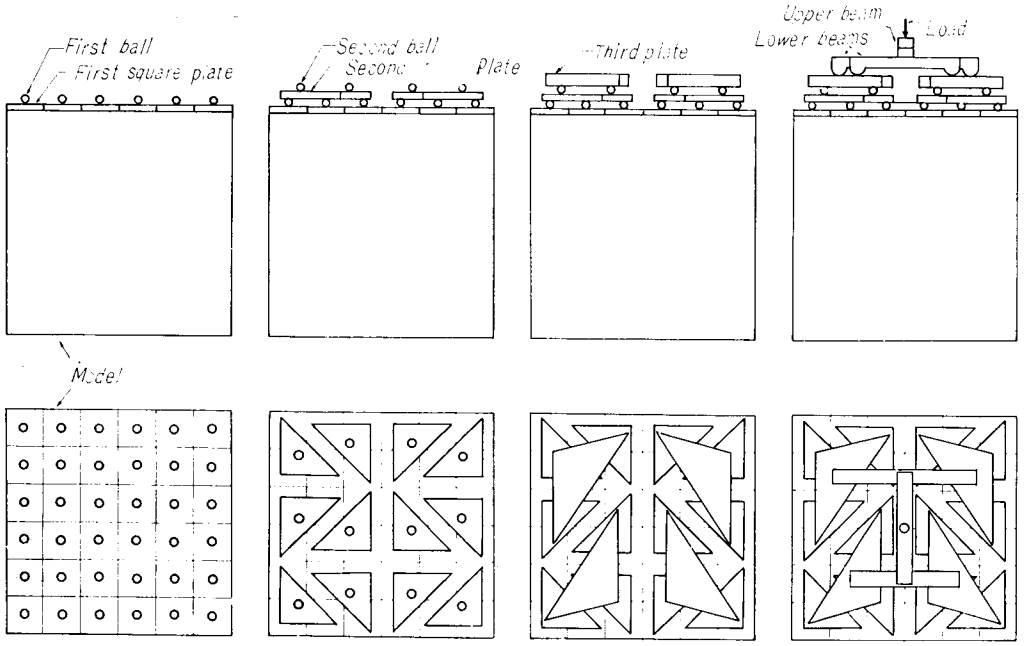

Fig. 7. Diagrams illustrating the method of loading.

Loading. Loading was produced in the following manner. The first model was loaded uniformly on the upper surface, the second model on the side surface and the third model on the other side surface.

Since the surface to be loaded has a considerable area, much effort was made to achieve uniform loading. It was attained by dividing the surface into thirty six square sections and applying equal loads to them. Fig. 7 illustrates the method of loading. A square steel plate was placed on each section, at the center of which a steel ball was put, and a triangular steel plate was placed on each three balls. At the centroid of each triangle formed by the three balls, a second steel ball was put, and a second triangular steel plate was again placed on each three second balls. At the centroid of each triangle formed by the three second balls a third steel ball was put. There were four third steel balls. They were loaded equally by placing a steel bar on each two of the four balls, and by loading on the center of the upper bar which was bridged between the centers of the lower two bars.

In case there is a hole on the surface to be loaded, the load on the square section which covers a part of the hole must be reduced by an amount proportional to the missed area. Accordingly, the position of every steel ball must be altered. Fig. 8 illustrates the positions of all the balls in the case

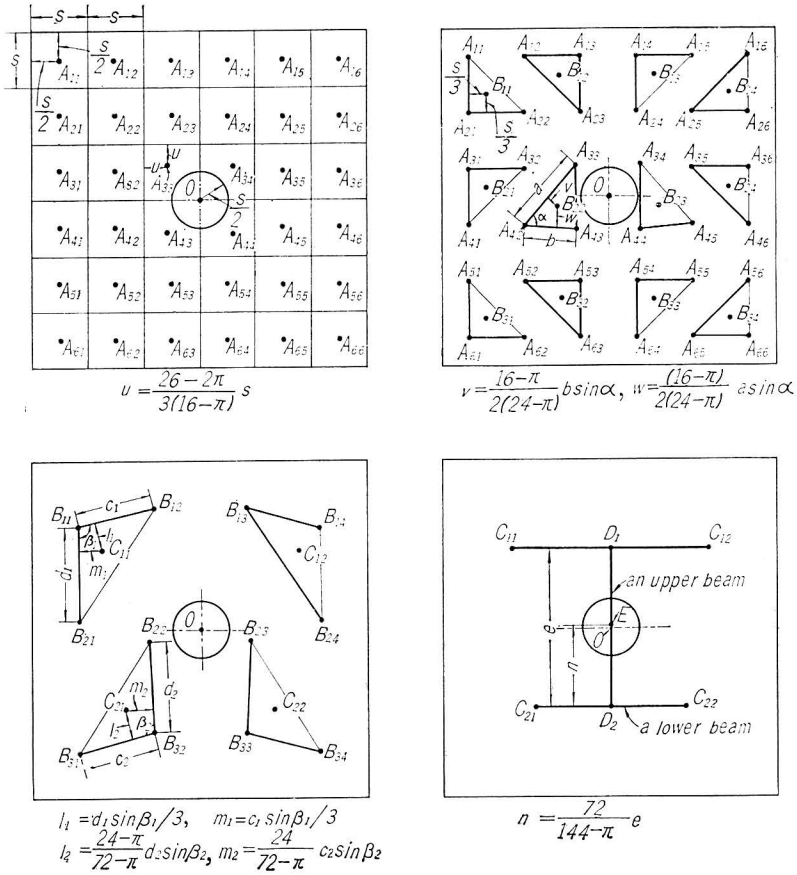

Fig. 8. Diagrams showing the position of every steel ball in case where there is a hole at the center of the surface to be loaded.

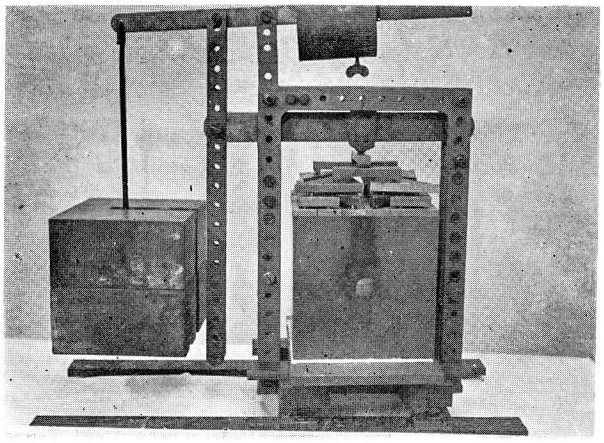

Fig. 9. The apparatus for loading.

where there is a circular hole whose diameter is s cm, one sixth the edge of the model. Let the load applied to Point E be P kg, then the uniform pressure applied on the surface of this model is $P/\{s^2(36-\pi/4)\}$ kg/cm^2.

The apparatus for loading consists of a frame, a double lever the magnification of which being 7.5, and weights, as shown in Fig. 9.

The pressure applied was 1.1, 1.65 or 2.2 kg/cm^2.

Fixing stress patterns. Every model that was being loaded was put into a thermostat furnished with an automatic regulator together with the loading apparatus as shown in Fig. 10, and heated at 130°C for a long time, say 24 hours, to secure uniform distribution of temperature. Then the temperature was lowered at a constant rate, −4°C/h, down to room temperature. In this way the stress pattern was fixed.

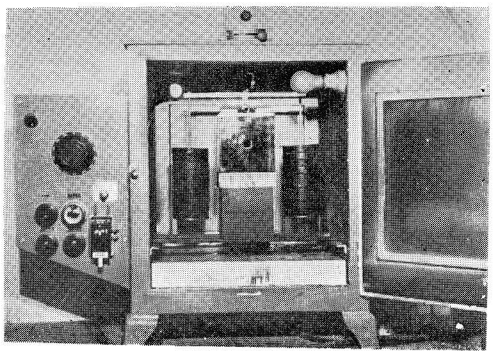

Fig. 10. The thermostat in which a model being loaded is placed.

The test piece for the sensitivity test was subjected to tensile stress by hanging a weight of 3 kg on it and the stress pattern was fixed.

Determination of stresses. Let us assume that the axes of the horizontal level and the vertical shaft coincide with the x- and z-axes, and the y-axis is perpendicular to both the x- and z-axes. Every model whose stress pattern was fixed was cut into many slices, about 3.5 mm thick, vertical to the x-, y- or z-axis, and the surfaces of them were polished. Then the stress patterns were observed through the slices, one by one, with a photoelastic polariscope set, immersing the slices in the liquid provided with one part of monobromonaphthalene-α and 0.59 parts of liquid paraffin in order to make the slices more transparent.

Much effort was exerted to determine the fringe order. Generally each fringe was counted from the fringe of zero order which was seen dark under an observation with a white light. When any fringe of zero order did not appear, one of the edges of a slice was cut aslant to yield a tapered surface, at the sharp edge of which a fringe of zero order was to be seen.

The principal stress difference at any point on a slice, $\sigma_1-\sigma_2$, is determined as a product of the fringe order of the point and the fringe stress, which was about 0.025 kg/mm in these experiments, divided by the thickness of the slice,

On a free surface, the principal stress normal to the surface is always zero. Therefore, if observation was made, for example, in the direction of σ_1, the value of $\sigma_1-\sigma_2$ determined from the fringe order gives directly the value of σ_2. We have frequently experienced, however, difficulty in deciding whether a stress under question is compressive or tensile. In such cases, several means were taken, e.g. another slice, parallel to the free surface, was taken, and it was observed with a photoelastic polariscope in the normal direction to determine $\sigma_1-\sigma_2$ for reference, or the slice was loaded and the variation in fringe order was observed, or the stresses in another model was fixed under the same condition, and the model was cut into slices in a different way to allow observation in other directions.

(2) **Results obtained and discussion**

The stress distributions on the inner surfaces of shaft bottom spaces in the three models for each type, one of them having been loaded in the x-direction, the other one in the y-direction and the last one in the z-direction, were determined in the way described above.

Fig. 11 shows the photographs of stress patterns observed in three slices of a model Type C, one containing the y- and z-axes and the other two the x- and z-axes.

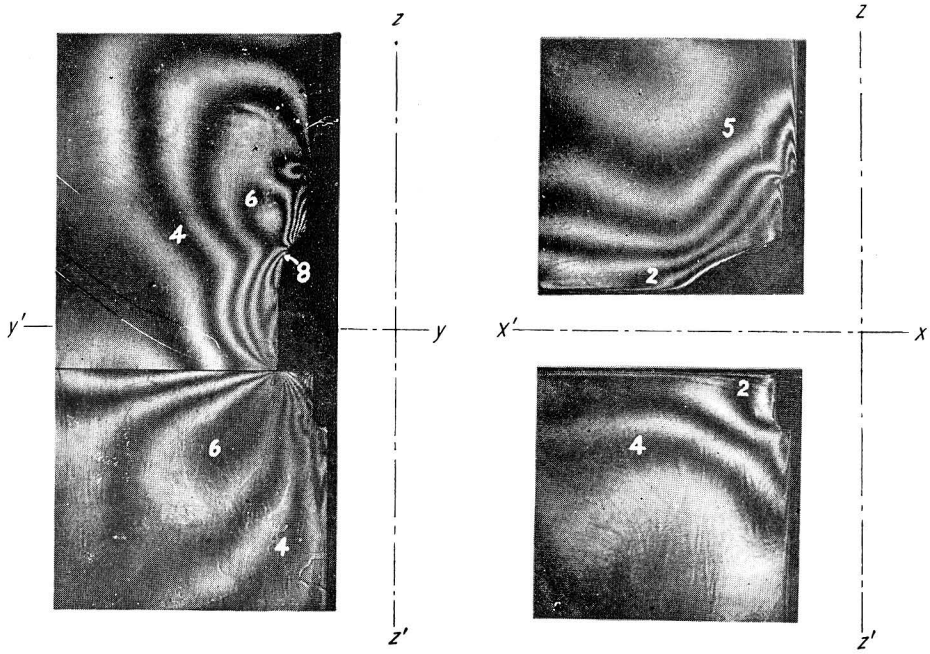

Fig. 11. Stress patterns observed through three slices of the Model Type C. (The numerals show the fringe orders.)

The important matter to be noticed here is that the stresses are statically indeterminate under three dimensional stress states. Consequently the values of stresses determined from photoelastic experiments have errors, which may be, in some cases, very serious. It will be very difficult to deduce the true values from the results of experiments. The authors have, however, attempted to correct the experimental results by referring to the analysis of stresses around a spherical opening in an elastic medium.

Assume that a spherical opening is made in a large cube of elastic material and define rectangular coordinates (x, y, z) and spherical coordinates (r, θ, ϕ) as shown in Fig. 12. When this cube is loaded in the direction of the z-axis with an intensity of p, the stress components σ_θ and σ_ϕ on the inner surface are given by the following equations[3]:

$$\left.\begin{aligned}(\sigma_\theta)_{\theta=0} &= (\sigma_\theta)_{\theta=\pi} = -\frac{3m+15}{2(7m-5)}p\,,\\ (\sigma_\theta)_{\theta=\pi/2} &= \frac{27m-15}{2(7m-5)}p\,,\\ (\sigma_\phi)_{\theta=\pi/2} &= \frac{15-3m}{2(7m-5)}p\,,\end{aligned}\right\} \qquad (3)$$

where m is the Poisson's number of the material. These equations show that $(\sigma_\theta)_{\theta=0,\frac{\pi}{2}}$ and $(\sigma_\phi)_{\theta=\pi/2}$ vary with the value of m as shown in Fig. 13.

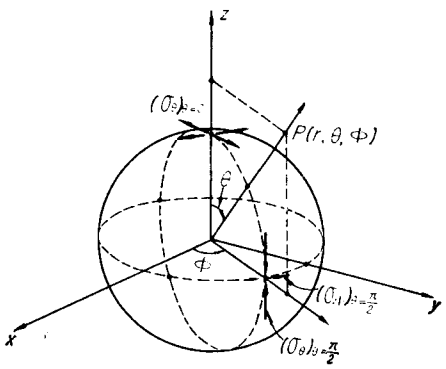

Fig. 12. A diagram showing a spherical opening, coordinates axes and some stress components.

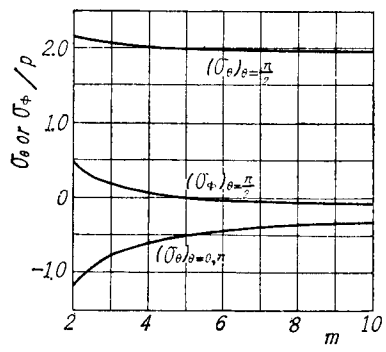

Fig. 13. The relation between the Poisson's number and the stress components σ_θ and σ_ϕ.

Considering that the Poisson's number of the material of the models used in the photoelastic experiments drops down to almost 2 when the stress patterns are fixed, and estimating the Poisson's number for rock is approximately 4, it is supposed, from the analysis described above, that we can take the magnitude of the true maximum tensile stress perpendicular to the direction

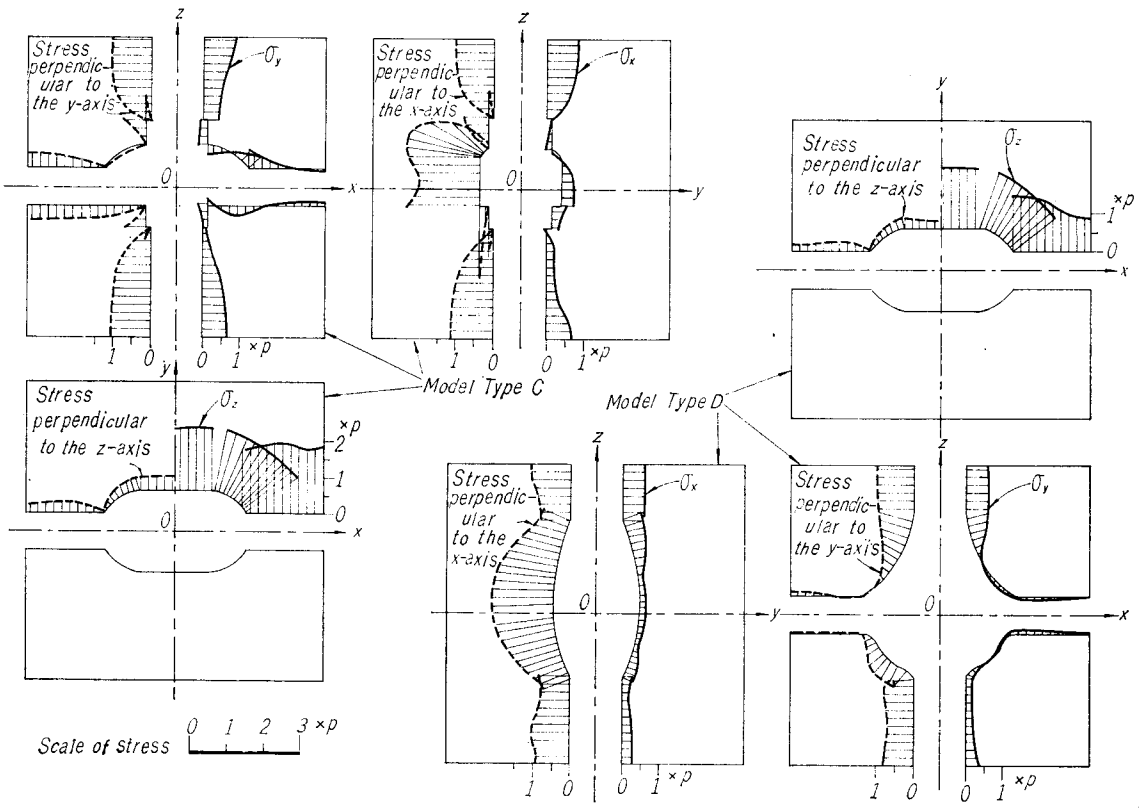

Fig. 14. The stress distributions on the inner surfaces of the Models Type C and D.

of loading to be a half of the value obtained from the experiment, while the true compressive stresses in and perpendicular to the direction of loading are equal to and are one seventh the experimental values respectively.

The stresses obtained from the photoelastic experiments were corrected by making use of the above mentioned relations. Then the stress distributions on the inner surface of the sections containing the x- and z-axes, the y- and z-axes and the x- and y-axes were determined assuming that the initial principal stresses were p in the z-direction and $p/3$ in the x- and y-directions. Fig. 14 illustrates the results. In this figure, the magnitude of the stress at any point is plotted on the normal to the inner surface drawn from the point, tensile stresses being inside of the opening and compressive stresses outside of it. On the left side of each section the stresses parallel to the section are plotted, while on the right side are the stresses normal to the section.

From this figure it is noticed that there appear considerable tensile stresses in the direction of the y-axis at such parts of the roof of a shaft bottom space

of Type C that are on the haulage level side, the maximum value being $-0.25\,p$ and appearing at the edge of the roof; that there appear also tensile stresses, though much smaller than the former, at the corresponding parts of the roof of the shaft bottom space of Type D, and that there appear maximum compressive stresses on the side walls of the shaft bottom spaces of both Types C and D, although they are not great, namely $2p$ for Type C and $1.6\,p$ for Type D.

These results show that the concentrated stresses around shaft bottom spaces are not so high as expected, and they decrease remarkably by rounding off the corners.

From the barodynamic experiments described in the preceding section, it has been learnt that if the rock was weak, the roof of the space was likely to fail owing to tension, and sometimes the side walls fell down by compression, and that the failure of rock due to tension was more likely to take place around shaft bottom spaces than around horizontal levels. Those conclusions can be well explained by the results of the photoelastic experiments.

According to the measurement of stress in the lining of the shaft bottom at Ooyubari Coal Mine, it was noted that the stresses at several points on the lining increased slowly with time, but tended towards certain limits, and that the rate of increase was greater on the roof than on other parts[4]. The rock around the shaft was weak shale, named Horokabetsu Shale, its compressive strength being about 400 kg/cm^2, and the depth of the shaft bottom was about 760 m. Although the conditions were not favorable, it has been ascertained that the lining has not been damaged for several years except for a few very small cracks. Those experiences are also explained by referring to the results of the present investigations.

4. Conclusion

The stress and the earth pressure phenomena around shaft bottom spaces with a few special shapes have been investigated by barodynamics and photoelastic experiments. Collecting the results of both experiments and considering the results of measurement of the stress in a shaft lining previously carried out, the following conclusion has been drawn.

It is possible that on the roof of a shaft bottom space there appear some tensile stresses, and on the side walls considerable compressive stresses. Therefore, if the rock is not sufficiently strong, it will fail at those parts. However, the maximum tensile stress as well as the maximum compressive stress is not very great. Therefore, in solid rock of high or medium strength,

the shaft bottom spaces will be maintained without any support. In stratified rocks, especially when the space is large or the depth is great, it is possible that the roof or sides of the space will fail. Therefore it will be necessary to line the space. As the failure of rock will not, probably, progress further once the corners are rounded off, the lining will not be required to be very thick.

References

1) Y. Hiramatsu and Y. Oka: Tech. Reps. of Eng. Res. Inst., Kyoto Univ., **11**, 65 (1961)
2) F. C. Johansen: Engineering, **129** (1929)
Bucky: A.I.M.E. Tech. Publ., **A-44** (1931)
E. Mikumo, Y. Hiramatsu and Y. Fujinaka: Journ. Min. Met. Inst. Japan, **76** (1952)
3) M. Kuranishi: Theory of elasticity, (1948)
4) Y. Hiramatsu and Y. Oka: THIS MEMOIRS, **23**, 90 (1961)